9

Point Automata Method for Dendritic Growth

Agnieszka Zuzanna Lorbiecka and Božidar Šarler
University of Nova Gorica
Slovenia

1. Introduction

Solidification microstructure is very important since it influences the properties of the final casting. Because of that has understanding and modelling of microstructures large industrial relevance. However, the understanding of solidification processes and related microstructures involves very complicated relationships. This is because it is affected by many interacting phenomena on different scales, such as heat and solute transfer, fluid flow, thermodynamics of interfaces and so on (Rettenmayr & Buchmann, 2006). Experiments that allow direct visualization of microstructure formation are difficult to perform. In the last decade, several numerical models, which can solve complicated transport phenomena and phase transformation under different boundary and initial conditions, were developed to calculate various microstructure features of solidifying materials such as grain growth with details of solidification interface morphology. Among of all numerical approaches Cellular Automata (CA) modeling (Wolfram, 2002) and phase field modeling (Qin & Wallach, 2003) are the most popular and widely used. We focus on the CA based approach in this chapter. A considerable progress on solidification microstructure simulation (Boettinger et al., 2000; Miodownik, 2002) has been made by the CA approach.

Rappaz and Gandin (Rappaz & Gandin, 1993) were the pioneering researchers who developed the CA model for modelling microstructure where the nucleation and the growth kinetics could be considered and grain structure with certain shapes and size were predicted. Gandin and Rappaz (Gandin & Rappaz, 1994; Gandin & Rappaz, 1997) simulated the grain structure by coupling the CA technique for the grain growth with the finite element method (FEM) solver for the heat flow (CA-FEM). Later Spittle and Brown (Spittle & Brown, 1995) coupled the CA with a finite difference solver (CA-FDM) for solute diffusion during the solidification of casting to predict the microstructure.

Unfortunately, the simple CA models for dendritic growth suffer from the strong impact of the anisotropy of the numerical grid. Consequences are that they tend to grow only in the grid direction (Zhan et al., 2008). It does not matter which crystallographic orientation will be chosen the CA method will always shift the dendrite with respect to the grid axis. During growth have the crystallographic orientation axes of different grains different divergence angles with respect to the coordinate system. In these cases is the growth stage difficult to simulate by the CA method. It is because the configuration of the CA mesh has a direct influence on simulated structure and shape. Anderson (Anderson et al., 1984) and later Spittle and Brown (Spittle & Brown, 1989) used a hexagonal, rather than the standard square 2-D lattice in order to better represent the grain anisotropy. But in general even now it is still

difficult to properly model the preferred crystallographic orientation. Rappaz and Gandin developed a decentered square method (Rappaz & Gandin, 1993) to try to solve this problem, which turns out to be very complicated.
We elaborate a novel Point Automata (PA) method in this chapter which follows the CA concept and is able to solve the mentioned crystallographic orientation problem. A basic feature of this method is to distribute nodes randomly in the domain instead of using regular cells, which leads to different distances between the nodes and different neighborhood configurations for each of them. This new approach was first proposed by Janssens for modelling the re-crystallisation (Janssens, 2000, 2003, 2010; Raabe et al., 2007). (Lorbiecka et al., 2009) were the first to couple the classical CA method with a meshless method instead of the FEM or FDM. They successfully predicted the grain structure in continuously cast steel billets. Subsequently, they replaced the CA method by the PA method in the same physical system (Lorbiecka & Šarler, 2009) and demonstrated the suitability of the PA method for cellular to equiaxed and equiaxed to cellular transition simulation in steel strands. The preliminary results of the dendritic growth based on the PA approach have been presented in (Lorbiecka & Šarler, 2009). This approach is explained and evaluated in details in the present chapter where we cope with a simple physical model which can simulate the dendritic forms during the solidification of pure metals from the undercooled melt. The developed algorithm is able to obtain the dendritic morphology by solving the heat transfer equation coupled with the solid fraction field evolution through the calculations of crystal growth velocity, interface curvature, thermodynamic and kinetic anisotropy, respectively.
The present chapter is structured in the following way: the CA and the PA methods are defined first, followed by the description of the governing equations of the heat transfer model and the stochastic model. The solution of temperature field and solid fraction is explained afterwards. The differences in numerical implementation of the classical CA and the new PA solution procedure are compared and discussed. The dendritic growth is simulated for two different orientations with the same random node arrangement with the PA method. Afterwards, the influence of two different random node arrangements as well as different node randomness was tested on two different crystallographic orientations. Finally, the numerical results are shown for seven dendrites growing simultaneously with the orientations 0° or 45° by the classical CA method and with different, more realistic orientations for the PA method. This demonstrates the flexibility of the new method for simulation of realistic dendritic structures. Conclusions with systematically listed characteristics of the PA method and future developments of the PA method complete the present chapter.

2. CA and PA definitions

Numerical models for solving the microstructure equations can briefly be divided into two categories: deterministic and stochastic (Stefanescu, 2009). Stochastic modelling represents a system where the physical phenomena are described by the random numbers. As a consequence the output data can vary from one simulation to another. The most popular stochastic methods used to simulate the microstructure formations are: Monte Carlo methods, Random Walker and CA approach. CA stochastic method (Wolfram, 2002) represents one of the numerical techniques, widely applied in modelling solidification and

re-crystallization processes. This algorithm was first established by Neumann (Neumann, 1987) and is nowadays commonly used in materials science. What follows are the basic elements of the CA method

- n-D (n=1, 2, 3) space is divided into a discrete number of n-dimensional elements which are named cells (polygons and polyhedrons).
- a state is assigned to each CA cell,
- the neighbourhood configuration is defined deterministic or stochastic for each CA cell,
- transition rules are defined which create a new state of the cell as a function of the states(s) of the cell(s) consisting of the previously defined local neighbourhood of the cell.

The above presented basic features of the CA system are commonly implemented in the literature. In the present work an alternative formulation to a common CA method is introduced. What follows are the basic elements of this novel PA method

- the starting point is to distribute PA nodes (not cells) randomly on the n-D computational domain,
- a state is assigned to each PA node,
- the neighbourhood configuration is defined for each node separately with respect to the chosen neighbourhood configuration,
- the neighbourhood of the node includes all random nodes whose positions are located in the domain of a circle in 2D or sphere in 3D. The number of the neighbours can vary locally. The transition rules are defined and they create a new state of the point as a function of the states(s) of the points(s) consisting the local neighbourhood configuration.

The irregular (also named random) PA cellular transitions rules can be used in exactly the same way as for the regular approach. In this sense the PA approach is not much different from the conventional one, despite bringing many advantages listed in the conclusions.

3. Governing equations

Thermally induced dendritic growth is considered in this example. It is physically described by the heat conduction and phase change kinetics. The temperature field is solved by the classical deterministic method and the phase change kinetics by the stochastic method.

3.1 Temperature field

Consider a two dimensional domain Ω with boundary Γ filled with a phase change material which consists of at least two phases, solid and liquid, separated by an interfacial region, which is usually very thin in pure substances. The thermal field in such a system is governed by the following equation (Xu et al., 2008)

$$\frac{\partial}{\partial t}(\rho h) = \nabla \cdot (\lambda \nabla T) \tag{1}$$

where ρ, h, λ, T represent material density, specific enthalpy, thermal conductivity and temperature, respectively. The specific enthalpy is constituted as

$$h = c_p T + f_l L \tag{2}$$

where c_p, L, f_l represent the specific heat, the latent heat and liquid fraction, respectively. All material properties are assumed constant for simulation simplicity. The solid and liquid fractions follow the rules

$$f_s + f_l = 1;\ f_s(T) = \begin{cases} 1 & for\ T \le T_s \\ \dfrac{T_l - T}{T_l - T_s} & for\ T_s < T < T_l \\ 0 & for\ T \ge T_l \end{cases} \tag{3}$$

where T_s, T_l, f_s represent the solidus temperature, liquidus temperature and the solid fraction, respectively. In case of a pure substance are the solidus and the liquidus temperature equal to the melting temperature T_m. However, for the computational purposes a narrow melting interval $T_l > T_m > T_s$ is always involved. The melting temperature T_m is defined as $T_m = \frac{1}{2}(T_s + T_l)$. We search for the temperature at time $t_0 + \Delta t$ by assuming the initial conditions

$$T(\mathbf{p}, t_0) = T_0(\mathbf{p});\ \mathbf{p} \in \Omega;\ f_s(\mathbf{p}, t_0) = f_{s0}(\mathbf{p});\ \mathbf{p} \in \Omega \tag{4}$$

(where $\mathbf{p}$ represents the position vector) and Neumann boundary conditions

$$\frac{\partial T}{\partial n}(\mathbf{p}, t) = F(\mathbf{p}, t);\ \mathbf{p} \in \Gamma,\ t_0 < t \le t_0 + \Delta t \tag{5}$$

where $\mathbf{n}$ represents the normal on Γ and T_0, f_{s0}, F represent known functions.

3.2 Phase change kinetics

3.2.1 Interface undercooling

The phase change situation can be achieved by undercooling a liquid below its melting temperature. When a solid seed is placed in such an undercooled melt, solidification will be initiated. Due to crystal anisotropy and perturbations in the system, the growth of the solid from the seed will not be uniform and an equiaxed dendritic crystal will form. Solid liquid interface is undercooled to the temperature T_f defined as (Saito et al., 1988; Nakagawa, et al., 2006)

$$T_f = T_m - \Gamma K \tag{6}$$

where Γ and K are the Gibbs-Thomson coefficient and the interface curvature, respectively.

3.2.2 Dendrite growth kinetics

The growth process is driven by the local undercooling. The interface growth velocity is given by the classical sharp model (Shin & Hong, 2002)

$$V_g^*(\mathbf{p}, t) = \mu_K\left(T_f - T(\mathbf{p}, t)\right);\ \mathbf{p} \in \Gamma_{s,l} \tag{7}$$

where V_g^*, μ_K, $\Gamma_{s,l}$ are the growth velocity, interface kinetics coefficient and the solid liquid interface, respectively.

Dendrites always grow in the specific crystallographic orientations. Therefore, it is necessary to consider anisotropy in either the interfacial kinetics or surface energy (or both). The present model accounts for the anisotropy in the both kinetics.

3.2.3 Thermodynamic anisotropy

The Gibbs-Thomson coefficient can be evaluated (Krane et al., 2009) by taking into account the thermodynamic anisotropy related to the crystal orientation and type as follows

$$\Gamma = \overline{\Gamma}\left[1 - \delta_t \cos\left[S\left(\theta - \theta_{def}\right)\right]\right] \tag{8}$$

where S, θ, θ_{def}, δ_t, $\overline{\Gamma}$ represent factors which control the number of preferential directions of the material's anisotropy ($S = 0$ for the isotropic case, $S = 4$ for four fold anisotropy and so on), growth angle (angle between the y coordinate and the line that connects the centre of the mass of the dendrite and point at $\Gamma_{s,l}$, see Fig. 1), the preferential crystallographic orientation, thermodynamic anisotropy coefficient and the average Gibbs-Thomson coefficient, respectively.

3.2.4 Kinetic anisotropy

The crystal growth velocity is calculated according to the crystal orientation by taking into the consideration the crystal growth direction θ and the preferred orientation θ_{def}. The crystal growth velocity follows the equation (Shin & Hong, 2002)

$$V = V_g^*(\mathbf{p}, t)\left[1 + \delta_k \cos\left(S\left(\theta - \theta_{def}\right)\right)\right] \tag{9}$$

where δ_k represents the degree of the kinetic anisotropy.

3.3 Coupling

The movement of the solid-liquid interface is governed by the evolution of the temperature field in the computational domain (Fig. 1).

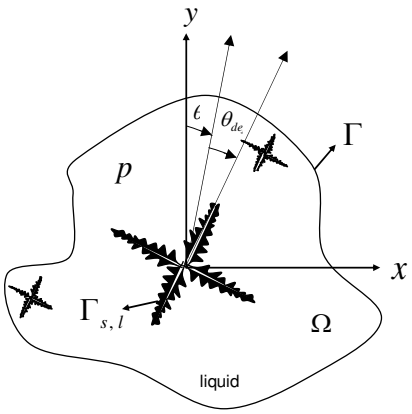

Fig. 1. Scheme of the dendritic growth

The dendritic structures are modelled by the stochastic method to track the interface motion coupled to the determinate heat transfer calculations. We first describe the solution of the temperature field based on the FDM method and subsequently the transition rules for the CA (PA) methods for calculation of solid fraction field. The flowchart of the calculations is given in Fig. 12.

4. Solution of the temperature field

A square domain is considered with length l. The number of points in FDM mesh in x and y directions is N. The total number of FDM grid points is N^2 - 4, since the four corner nodes are not considered.
A uniform FDM discretization is made with mesh distance $\Delta x = \Delta y = a = l/(N-1)$ as seen in Fig. 5 (left). The solution for the temperature field is performed by the simple explicit FDM. Solution of the temperature field in the domain nodes is thus

$$T_{i,j} = T_{0\,i,j} + \frac{\Delta t \lambda}{\rho c_p}\left(\left[\left(T_{0\,i-1,j} - 2T_{0\,i,j} + T_{0\,i+1,j}\right)/\left(\Delta x^2\right)\right] + \left[\left(T_{0\,i,j-1} - 2T_{0\,i,j} + T_{0\,i,j+1}\right)/\left(\Delta y^2\right)\right]\right) + \\ + \frac{L}{c_p}\left(f_{s\,i,j} - f_{0s\,i,j}\right) \tag{10}$$

for $i = 2,3,...,N-1$ and $j = 2,3,...,N-1$
The boundary nodes are calculated (the Neumann boundary conditions are set to $F = 0$ W/m²) as: west $T_{1,j} = T_{2,j}$ for $j = 2,...,N-1$, east $T_{N,j} = T_{N-1,j}$ for $j = 2,...,N-1$, north $T_{i,N} = T_{i,N-1}$ for $i = 2,...,N-1$ and south $T_{i,1} = T_{i,2}$ for $i = 2,...,N-1$, where Δt, $f_{0s\,i,j}$, $T_{0\,i,j}$, $T_{0\,i+1,j}$, $T_{0\,i-1,j}$, $T_{0\,i,j+1}$, $T_{0\,i,j-1}$ are the time step, initial solid fraction, initial temperature in the FDM central, east, west, north and south nodes, respectively.

5. Solution of the solid fraction field

We now define and discuss the elements of the classical CA and the novel PA methods in details.

5.1 Definition of mesh and neighbourhood configuration

Square cells with length $\Delta x = \Delta y = a = l/n$ where $n = N-1$ represents the number of cells in x and y directions are considering in the CA approach. In the PA approach the square is divided in uniform or nonuniformy distributed nodes. Cells are not defined.

5.1.1 Mesh and neighbourhood in the CA method

A basic definition of neighborhood originates from the classical CA approach which operates on the grid divided into the square cells (Neumann, 1987; Nastac, 2004). The cell structure is depicted in Fig. 2. In our calculations the Neumann configuration which takes into account only the closest neighbor's cells during the computation is applied.
The conventional square mesh structure is commonly applied in the CA calculations. It represents a square domain covered by the CA cells $x_{CA\,i,j}, y_{CA\,i,j}$ located exactly in the middle of four FDM nodes, as it is depicted in Fig. 5 (left).

$$x_{CA\,i,j} = \frac{1}{2}\left[x_{FDM\,i,j} + x_{FDM\,i+1,j}\right]; \quad y_{CA\,i,j} = \frac{1}{2}\left[y_{FDM\,i,j} + y_{FDM\,i,j+1}\right] \tag{11}$$

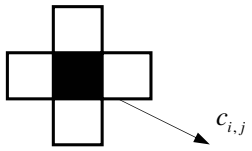

$$c_{i,j} = \left\{c_{i+1,j}, c_{i,j+1}, c_{i-1,j}, c_{i,j-1}\right\}$$

Fig. 2. Graphical representation of the Neumann neighbourhood configuration for the conventional CA method

5.1.2 Mesh and neighborhood in the PA method

The PA node grows with respect to the heat flow and with respect to the 'neighbourhood' configuration which is now associated with the position of the neighbouring PA nodes which fall into a circle (Janssens, 2000, 2003) with radius R_H in 2-D or a sphere in 3-D. It means that each PA node can in case of the random mesh contain different number and position of the neighbours, which give various possibilities of neighbourhood configurations for each node. For the novel PA method the random node arrangement is in the present chapter generated from the regular CA mesh.

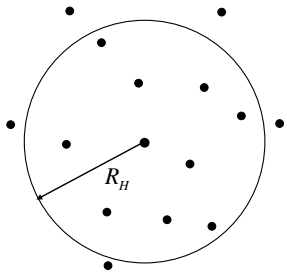

$$c_{i,j} = \left\{c_{i,j}; \left|r_i - r_j\right|_{i \neq j} < R_H\right\}$$

Fig. 3. Graphical representation of the neighbourhood configuration proposed for the new PA method

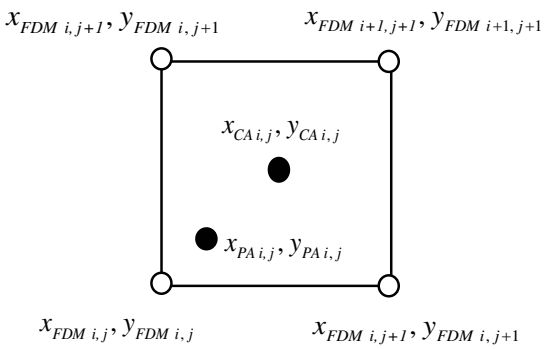

Fig. 4. Schematic representation of the relationship between FDM nodes (4 corners), CA cell (center) and the random PA node

To construct the random node arrangements, the CA cell centres are displaced to the randomly chosen positions and become random PA nodes $x_{PA\,i,j}$, $y_{PA\,i,j}$ on the computational domain (see Fig. 5 bottom).
The displacement of each CA centre is assumed only in the square area limited by the four FDM nodes. The following procedure is applied

$$x_{PA\,i,j} = x_{CA\,i,j} + \varepsilon\left[2rand - 1\right];\;\; y_{PA\,i,j} = y_{PA\,i,j} + \varepsilon\left[2rand - 1\right] \tag{12}$$

where $x_{PA_{i,j}}$, $y_{PA_{i,j}}$, ε represent coordinates of PA nodes and the scaling value $0 \le \varepsilon \le 0.49$, respectively. It must be emphasized that the PA procedure is established on the random nodes in general. The heat transfer calculations are performed on the regular FDM nodes, which is explained in Section 6.

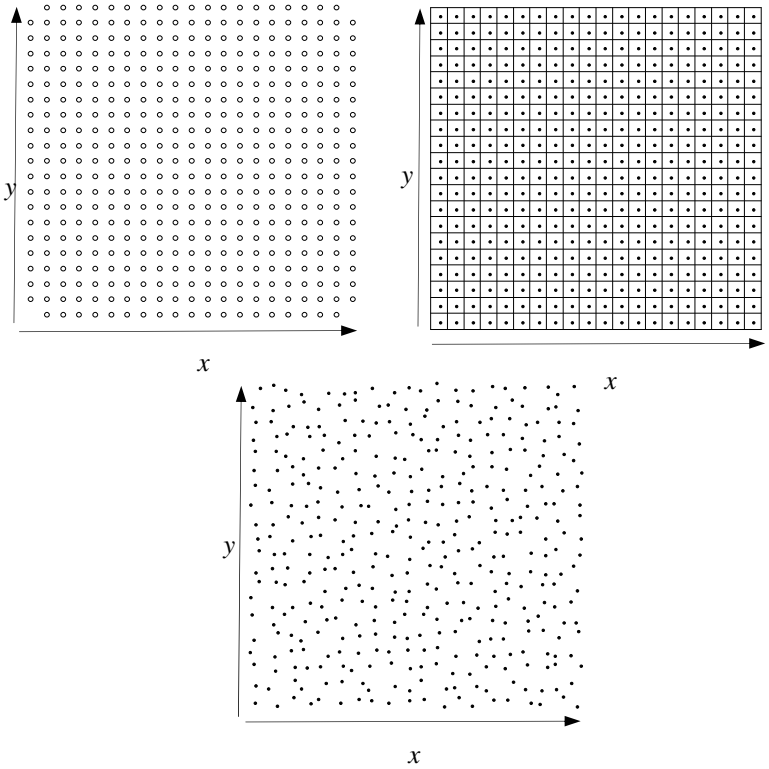

Fig. 5. Scheme of the space discretization: (top left) FDM nodes with $N = 21$, (top-right), CA cells with $n = 20$, (bottom) PA nodes with $n = 20$

5.2 Curvature calculations

The interface curvature is approximated by the counting cell procedure developed by Sasikumar and Sreenivasan (Sasikumar & Sreenivasan, 1994).

5.2.1 Calculation of curvature in the CA method

The expression for curvature K is given by the formula (Krane et al., 2009)

$$K = \frac{1}{a}\left(1 - \frac{2N_{s\,CA}}{N_{t\,CA}}\right) \tag{13}$$

where $N_{s\,CA}$ and $N_{t\,CA}$ are the number of solid CA cells whose centres fall inside the circle of assumed radius R_c and the total number of CA cells whose centres fall inside the circle, respectively (see Fig. 6 (top)).

5.2.2 Calculation of curvature in the PA method

The expression for PA is derived from the expression for the CA method (equation 13) by assuming the average node distance $\bar{a}$ instead of a (see Fig. 6 (bottom)).

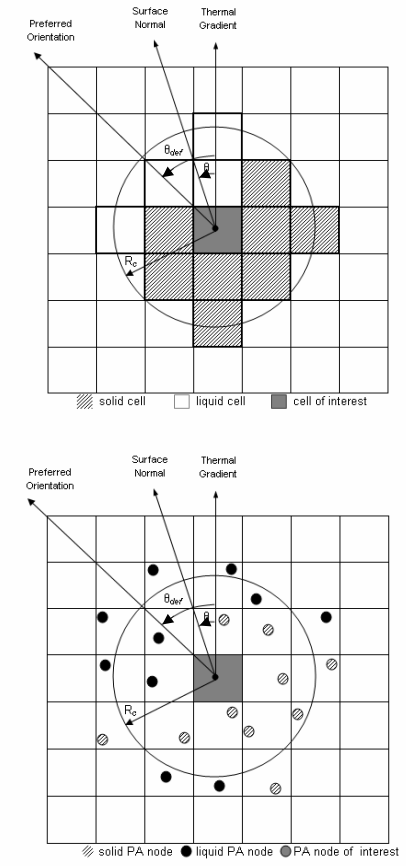

Fig. 6. Top: scheme showing a circle sample with $R_c = 2a$ for calculating the curvature in the conventional CA method (example: $N_{s\,CA} = 8$ and $N_{t\,CA} = 12$); bottom: in the PA method (example: $N_{s\,PA} = 7$ and $N_{t\,PA} = 11$)

5.3 Phase change

The crystal growth velocity is calculated according to the crystal orientation. The envelope of the grain can be expressed by the equation 9 which is depicted in Fig. 7.

Once a CA cell (or PA node) becomes solid it starts to grow with respect to the 'neighbourhood' configuration (see Fig. 2 and Fig. 3). Each of the CA cells (or the random nodes) can have two possible states: liquid or solid. The CA cell (or PA node) becomes solid through the growth process. The change of the solid fraction of the CA cell or PA node is calculated from the crystal growth velocity.

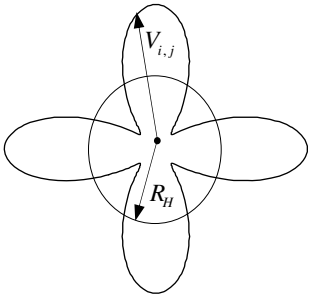

Fig. 7. Schematic representation of the shape function (for parameters see Table 1)

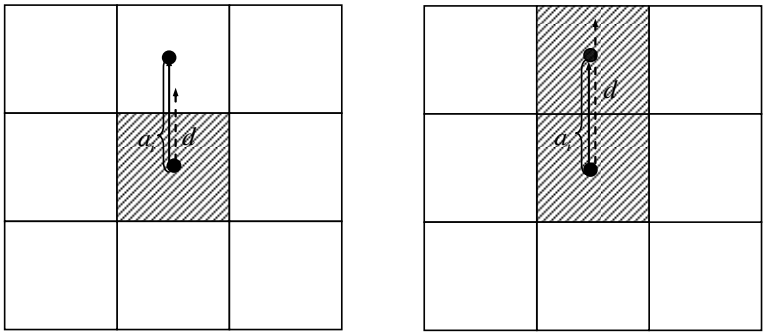

Fig. 8. Left: growth front will not reach the closest neighbour $d < a_i$. The CA cell will not be converted to solid (example for the Neumann neighbourhood configuration); left: growth front will reach the closest neighbour $d \geq a_i$. The CA cell will be converted to solid (example for the Neumann neighbourhood configuration)

For all neighbours of the treated solid CA cell (or solid PA node), general criterion d is checked which is represented by the following formula

$$d = \frac{l(t)}{a_i} \tag{14}$$

$$l = \int_{t_0}^{t} V_{i,j}\, dt \tag{15}$$

where a_i represent lengths from the analyzed CA cell or PA node to the nearest one.
If neighbour is one of the four nearest east, north, west, south neighbours then in the CA method this distance becomes $a_i = a$. In the PA method a_i $(a_i < R_H)$ represents the different distances to the neighbouring PA nodes which fall into the circle with radius R_H (see Fig. 9).
When $d \geq a$ or $d \geq a_i$ (Fig. 8 (right) and Fig. 9 (right)) the growing solid touches the centre of the neighbouring CA cell or PA node and this cell/node transforms its state from liquid to solid $f_{s\,PA} = 1$.

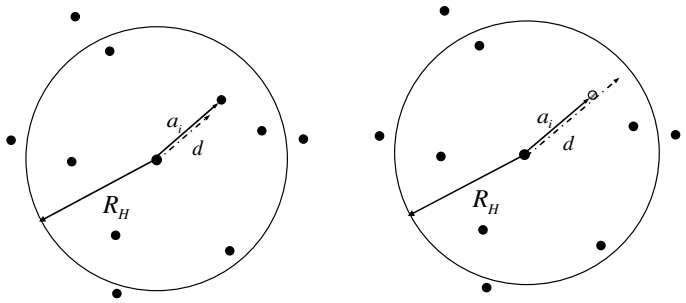

Fig. 9. Left: growth front will not reach the closest neighbour $d < a_i$. The PA node will not be converted to solid; right: growth front will reach the closest neighbour $d \geq a_i$. The PA node will be converted to solid

6. FDM-PA-FDM transfer of temperature and solid fraction

6.1 FDM-PA transfer of temperature

The obtained values of temperature on regular FDM grid (see Section 4) are in each time step transferred to random PA grid according to the described scheme (Fig. 12). The following simple interpolation formula (Xu & Liu, 2001) is used in the present chapter

$$T_{PA\,i,j} = \left(T_{i,j+1}l_1 + T_{i+1,j+1}l_2 + T_{i+1,j}l_3 + T_{i,j}l_4\right) / \sum_{i=1}^{4} l_i \tag{16}$$

In case of FDM-CA the equation 16 reduces to

$$T_{CA\,i,j} = \left(T_{i,j+1} + T_{i+1,j+1} + T_{i+1,j} + T_{i,j}\right) / 4 \tag{17}$$

where $T_{PA\,i,j}$, $T_{i,j}$, $T_{CA\,i,j}$ and l_i represent the temperature of the PA node, the temperatures of the four closest FDM nodes, the temperature for the centre CA cell and the distances to the nearest four FDM nodes, respectively. The calculation is repeated in each time step (see Fig. 10).

6.2 PA-FDM transfer of solid fraction

The temperature field at time $t_0 + \Delta t$ can be calculated from the equation 10 for all FDM nodes. Then these values are recalculated to all PA nodes according to the equation 16. Afterwards the PA procedure takes place (see Section 3). The output information from this

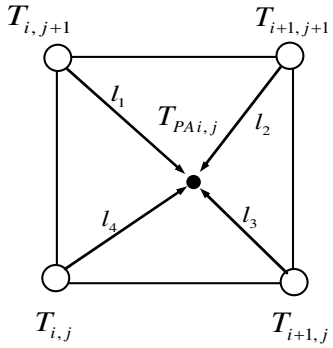

Fig. 10. Relationship between four FDM nodes and PA node for the calculation of the temperature values

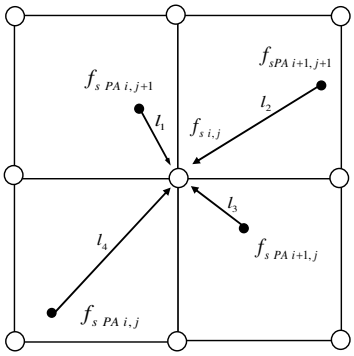

Fig. 11. Relationship between the FDM node and four neighbouring PA nodes for the transfer of solid fraction

level of calculation is the value of solid fraction for all random PA nodes $f_{s\,PA\,i,j}$ which have to be transferred to the FDM nodes to be able to calculate the new values of temperature (Fig. 11). The following equation is applied

$$f_{s\,i,j} = (f_{s\,PA\,i,j+1}\,l_1 + f_{s\,PA\,i+1,j+1}\,l_2 + f_{s\,PA\,i+1,j}\,l_3 + f_{s\,PA\,i,j}\,l_4) / \sum_{i=1}^{4} l_i \tag{18}$$

In case of FDM-CA the equation 18 reduces to

$$T_{CA\,i,j} = \left(T_{i,j+1} + T_{i+1,j+1} + T_{i+1,j} + T_{i,j}\right) / 4 \tag{19}$$

where $f_{s\,i,j}$ and $f_{s\,PA}$ represent the solid fraction for the FDM nodes and for the PA nodes, respectively.

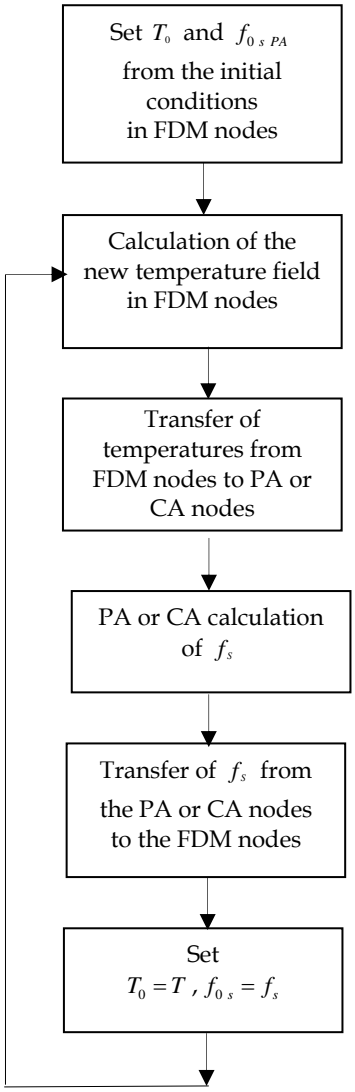

Fig. 12. Flowchart of the thermal field and solid fraction calculations

7. Numerical example

7.1 Numerical implementation

The model was coded in Fortran. For the dendritic growth in Figs. 13-17, the CPU time varies from 10 to 15 minutes depending on the input data. The solid PA nodes or CA cells are depicted by a colour pixel which can be observed on the screen during the simulation.

7.2 Problem definition and distretization

Initial conditions. Simplified material properties presented in Table 1 for pure aluminium (Kammer, 1999) are used in all prepared numerical examples. The process starts from the predetermined solid seed position in one single PA or CA node in the middle of the computational domain with the following initial conditions of temperature $933.45\,\mathrm{K} - 1.5\,\mathrm{K}$ and solid fraction $f_s = 1$. All other PA nodes are assumed to be liquid $f_s = 0$ and FDM nodes with the temperature $770.23\,\mathrm{K}$. This data is constant with the problem defined in the article. The numerical examples in the present chapter are solved by the FDM based temperature calculations and CA or PA based solid fraction calculations. The computational domain is the square with length $l = 350$ μm and uniform discretization $N = 701$.

Mesh generation. FDM and CA methods are always constructed on a regular node arrangement in the present chapter. In the PA approach the random node arrangement needs to be constructed. The PA approach was tested first with the predetermined node arrangement PA-(A), see Fig. 14 and then with different types of random node arrangements: PA-(B), PA-(C), see Fig. 15, respectively (Table 2).

Time step. The time step used in FDM calculation of the temperature field is limited by the formula (Zhu & Hong, 2001)

$$\Delta t_{FDM} = \frac{a^2}{4.5D};\ D = \frac{\lambda}{\rho c_p} \tag{20}$$

where D represents the thermal diffusivity. For the calculations of the solid fraction field by the CA and PA method the following relation is used (Daming et al., 2004) for assuming stability

$$\Delta t_{CA} = \eta \min\left(\frac{a}{V^*_{\max}}, \frac{a^2}{D}\right) \tag{21}$$

where η and $V^*_{\max}$ represent the positive constant less then 1 and the maximum growth velocity of all interface cells, respectively.

For the stability of the coupled FDM-CA-PA procedure a minimum of Δt_{CA} and Δt_{FDM} should be used. All depicted results of simulations are shown for the different crystallographic angles after 1500 time steps of the length $\Delta t_{FDM} = 6.82x10^{-10}$ s.

Thermal fluctuations. In order to avoid the symmetric shape of the dendrite (in the conventional CA approach) some fluctuations need to be introduced into the calculations. The following equation is commonly applied $P = 1 + \lambda^* rand$. Thermal noises are usually present by putting the random fluctuations F into the calculations of the latent heat, undercooling temperature or velocity (Voller, 2008). It this chapter we use them in the velocity calculations $V = V$ x P.

Neighbourhood configuration. In the CA approach only the closest neighbourhood configuration has been analyzed. Larger the value of R_H is chosen in the PA method more dendritic and irregular structures can be observed. A more extended area of neighbours needs to be taken into the consideration in the PA method. The radius of neighbourhood should be kept at a minimum of 1.5 μm in case of $a = 0.5\,\mu$m. For smaller values the dendritic shapes become distorted and the preferred orientations lost as well.

Symbol	Value	Unit
ρ	2700	kg/m^3
T_m	933.45	K
T_s	933.45-1.5	K
T_l	933.45+1.5	K
λ	210	W/mK
c_p	955.56	J/kgK
L	259259.26	J/kg
η	0.222	1
$\overline{\Gamma}$	1.6 x 10^{-7}	Km
δ_t	0.3	1
δ_k	0.75	1
S	4	1
R_c	1.5	μm
R_H	2	μm
μ_K	2	m/sK
l	350	μm
n	700	PA nodes/ CA cells
N	701	FDM nodes

Table 2. Nominal parameters used in the calculations

7.3 Simulated results

The dendritic morphologies were calculated by the classical FDM-CA and the novel FDM-PA approaches. The following numerical examples were prepared

- From CASE 1 to CASE 2 the dendritic growth process is simulated by the PA method with the same random node arrangement denoted (PA-(A)) for the following two orientations $\theta_{def} = 22^\circ$ and $\theta_{def} = 37^\circ$.
- From CASE 3 to CASE 4 the dendritic growth process is simulated by the PA method with different random node arrangements (PA-(B), PA-(C)) for the orientation $\theta_{def} = 10^\circ$.
- From CASE 5 to CASE 6 the dendritic growth process is simulated by the PA method with different randomness of the node arrangement $\varepsilon = 0.10$ and $\varepsilon = 0.49$, for the orientation $\theta_{def} = 8^\circ$.
- From CASE 7 to CASE 8 the dendritic growth process is simulated by the PA method including the factor responsible for the correction in the lengths of the x and y branches for different random node arrangements (PA-(F)-F, PA-(G)-F).

The results have been arranged and represented in the following way. Fig. 13 represents seven dendrites growing simultaneously at orientations 0° and 45° as the grid is constructed by the classical FDM-CA method. The FDM-PA calculations with different orientations of the crystallographic axis are depicted in Fig. 14 based on the same node

arrangement. Then Fig. 15 shows the FDM-PA results with the varied random mesh structure for a single dendrite with orientation $\theta_{def} = 10°$. Fig. 16 represents dendritic growth for a single dendrite with $\theta_{def} = 8°$ for a different node arrangement randomness. In Fig. 17 the results for the PA method, where the randomness correction factor is applied, are represented (see discussion in the next paragraph). Finally, Fig. 18 represents seven dendrites growing simultaneously at different orientations by the FDM-PA method.

CASE	θ_{def}	λ^*	ε	node arrangement
1	22°	0	0.49	PA-(A)
2	37°	0	0.49	PA-(A)
3	10°	0	0.49	PA-(B)
4	10°	0	0.49	PA-(C)
5	8°	0	0.49	PA-(D)
6	8°	0	0.10	PA-(E)
7	0°	0	0.49	PA-(F)-F
8	0°	0	0.49	PA-(G)-F

Table 1. Parameters used in the calculations

7.4 Discussion of the results

The orientations of crystallographic axes of different dendrites have different orientations in general. It is commonly recognized that this process is difficult to simulate by the classical CA method since the dendrite will always switch to 0° or 45° direction during the growth. Our testing is thus primarily focused on the growth of the dendrite at different orientations by the novel PA method. Simulated examples are for the random node arrangements PA-(A),…, PA-(F) presented in Figs. 14-17, respectively. They show that when employing the PA method any of the crystallographic orientation can easily be achieved. Results show that the proper growth direction is always observed with increasingly random ($\varepsilon \to 0.49$) node arrangement.

For the same input parameters the dendritic growth process simulated by the CA and PA method for the $\theta_{def} = 0^\circ$ preferential crystallographic orientation gives the different lengths of x and y branches. This is due to the influence of the random node arrangement and subsequent variable distances between the nodes. In the CA method the same value of a is taken while for the PA method this distances are different and might vary between maximum $\Delta x = \Delta y = 2\varepsilon a$ and minimum $\Delta x = \Delta y = 2(1-\varepsilon)a$.

It can be concluded that the differences in the length between x and y directions with respect to the random node arrangement are almost constant and kept below $\approx 5\%$.

The average length of the dendrite at ten different orientations and some random node arrangement with $\varepsilon = 0.49$ is 152.8 ± 5.18 μm. The average length of the dendrite calculated

with four different random node arrangement for the fixed angles 5°, 15° and 30° is 153.37 ± 5.39 μm, 156.12 ± 6.44 μm and 151.75 ± 5.36 μm, respectively (Lorbiecka & Šarler, 2010). From this one can conclude that the errors caused by the rotation of the dendrite are at the same order as the errors cussed by different random node arrangements. Fig. 16 demonstrates that when reducing ε from 0.49 to 0.1 the PA starts to behave like the CA and the proper simulation of the dendrite is not possible. We are too close to the classical node structure in such case and CA limitations appear.

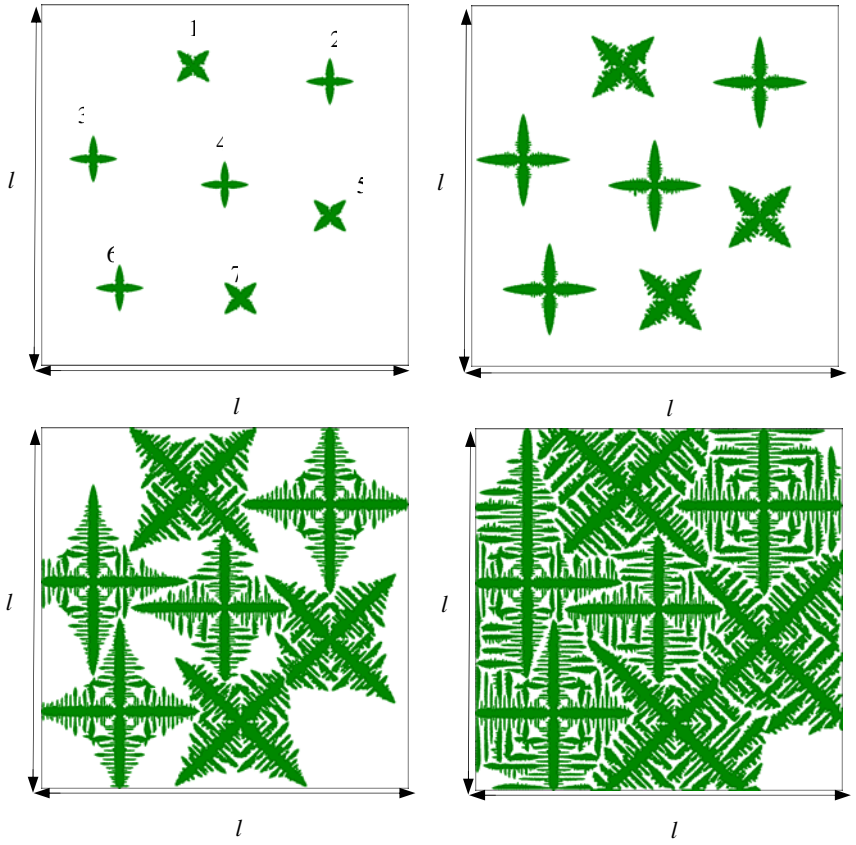

Fig. 13. Seven dendrites growing simultaneously at orientations 0° and 45° after 350, 700, 1500 and 2500 time steps of the length 6.82×10^{-10} s. FDM-CA solution procedure

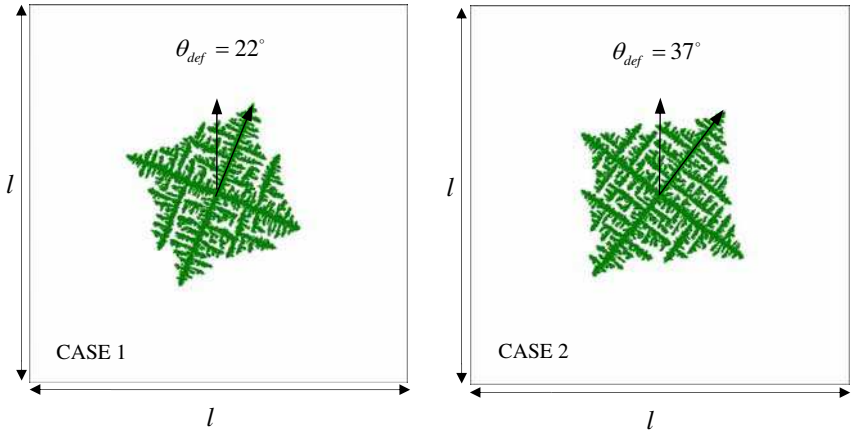

Fig. 14. Simulated dendritic growth for a single dendrite for two orientations by the PA method for the same PA-(A) random node arrangement $\theta_{def} = 22°$ and $\theta_{def} = 37°$

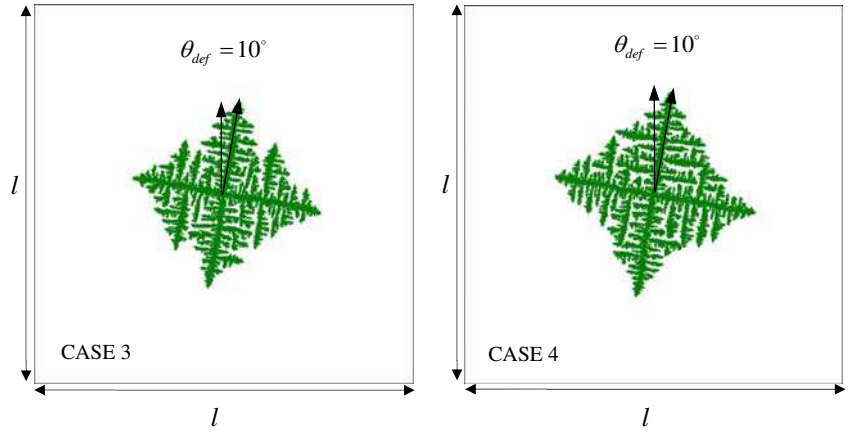

Fig. 15. Simulated dendritic growth for a single dendrite with $\theta_{def} = 10°$ for different random node arrangement structures: PA-(B), PA-(C), respectively

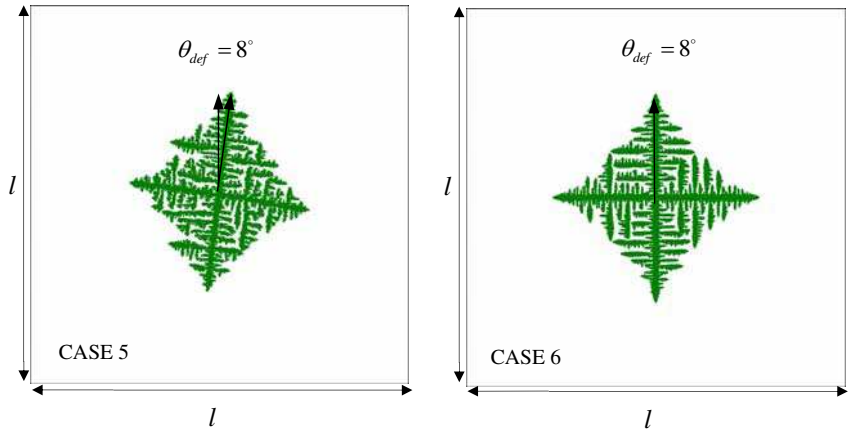

Fig. 16. Simulated dendritic growth for a single dendrite with $\theta_{def} = 8^{\circ}$ for different node arrangement randomness $\varepsilon = 0.49$ PA-(D) and $\varepsilon = 0.1$ PA-(E).

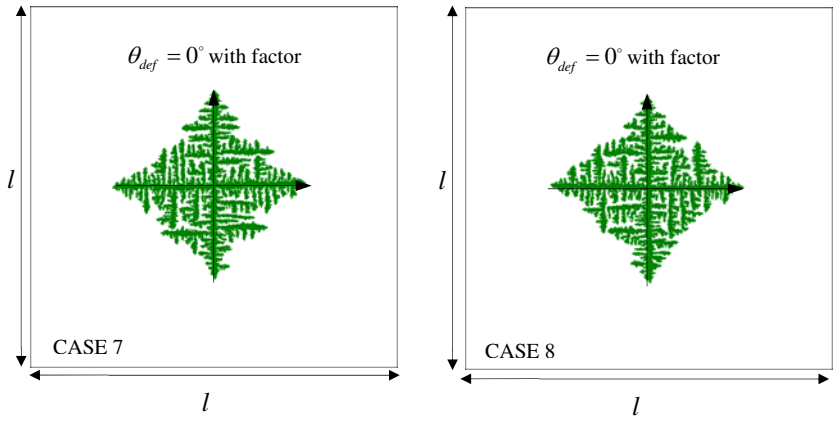

Fig. 17. Simulated dendritic growth for a single dendrite by the PA method with factor 1.25

To achieve the same dendrite length in PA method as in the CA method, an empirical factor, which multiplies the calculated velocity in the PA method, was added in the code. It can be shown that putting factor 1.25, (for the random node arrangement ε = 0.49) in the PA calculations, the branches will have the same length in both methods (see Fig. 17).

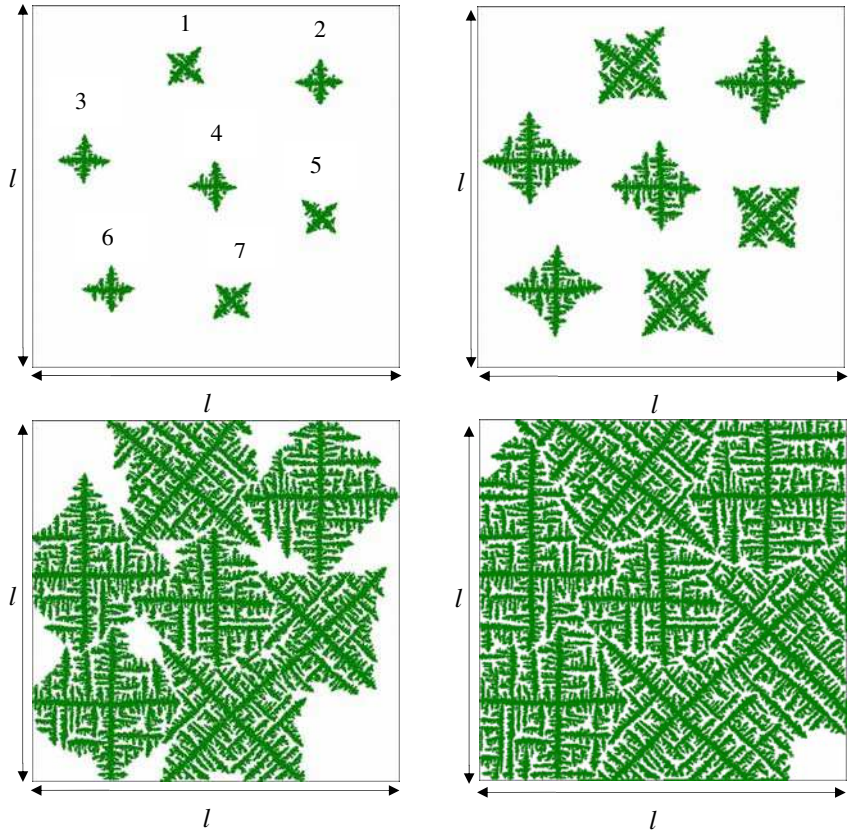

Fig. 18. Seven dendrites growing simultaneously at different orientations after 350, 700, 1500 and 2500 time steps of the length 6.82×10^{-10} s. FDM-PA solution procedure

In the present study it is not necessary to put any thermal fluctuations in the PA method. The random node arrangements in the PA method replace the thermal fluctuations of the CA method.

8. Conclusions

In this chapter a novel PA method is developed and applied to model the dendritic growth process. The principal characteristics and advantages of the developed PA method are

- No need for mesh generation or polygonisation. Only the node arrangement has to be generated, but without any geometrical connection between nodes.
- In the new PA method the governing equations are solved with respect to the location of points (not polygons) on the computational domain.
- The random grid PA method allows to rotate dendrites in any direction since it has a limited anisotropy of the node arrangements.
- PA method offers a simple and powerful approach of CA type simulations. It was shown that both methods are able to qualitatively and quantitatively model a diverse range of solidification phenomena in almost the same calculation time.
- The dimension of the neighborhood radius and generation of the random node arrangement has to be chosen carefully in order to be able to rotate the dendrite.
- Straightforward node refinement possibility.
- Straightforward extension to 3-D.

The use of FDM-PA method instead of FDM-CA method implies transfer of the results from the regular FDM mesh to the irregular PA node arrangements and vice versa. This is not the case in the classical FDM-CA method. A replacement of the FDM method with a meshless (Atluri, 2004; Liu & Gu, 2005; Šarler et al., 2005; Šarler & Vertnik, 2006) method that is able to directly cope with irregular node arrangement is underway.

9. Acknowledgment

The first author would like to thank the EU Marie Curie Research Training Network INSPIRE for position to study and research at the University of Nova Gorica, Slovenia. The second author would like to thank the Slovenian Research Agency for funding in the framework of the project J2-0099 Multiscale modelling of liquid-solid systems.

10. Reference

Atluri, S.N. (2004). The Meshless Method (MLPG) for Domain and BIE Discretization, Tech Science Press, Forsyth

Anderson, M.P.; Srolovitz, D.J. & Grest, S.G. (1984). Computer simulation of grain growth. I. Kinetics. *Acta Metall*, Vol.32, pp. 783-791

Boettinger, W.J.; Coriell, S.R.; Greer, A.L.; Karma, A.; Kurz, A.; Rappaz, M. & Trivedi, R. (2000). Solidification microstructure recent developments, future directions. *Acta Metall.*, Vol.48, pp. 43-70

Daming, L.; Ruo, L. & Zhang, P. (2004). A new coupled model for alloy solidification. *Science in China Ser. A. Mathematics.*, Vol. 47, pp. 41-52

Gandin, Ch.A. & Rappaz, M. (1994). A coupled finite element-cellular automaton model for the prediction of dendritic grain structures in solidification processes. *Acta Metall.*, Vol.42, No.7, pp. 2133-2246

Gandin, Ch.A. & Rappaz, M. (1997). A 3D cellular automaton algorithm for the prediction of dendritic grain growth. *Acta Metall.*, Vol. 45, pp. 2187-2195.

Janssens, K.G.F. (2000). *Irregular cellular automata modeling of grain growth.* Continuum Scale Simulation of Engineering Materials, Germany

Janssens, K.G.F. (2003). Random Grid, Three Dimensional, Space-Time Coupled Cellular Automata for the Simulation of Recrystallization and Grain Growth. *Modelling Simul. Mater. Sci. Eng*, Vol.11, No.2, pp.157-171

Janssens, K.G.F.; Raabe, D.; Kozeschnik, E.; Miodownik, M.A. & Nestler, B. (2007). *Computational Materials Engineering*, Elsevier Academic Press, Great Britain

Janssens, K.G.F. (2010). An introductory review of cellular automata modeling of moving grain boundaries in polycrystalline materials. *Mathematics and Computers in Simulations,* Vol.80, No.7, pp. 1361-1381

Krane, M.J.M.; Johnson, D.R. & Raghavan, S. (2009). The development of a cellular automaton - finite volume model for dendritic growth. *Applied Mathematical Modelling*, Vol.33, No.5, pp. 2234-2247

Kammer, K. (1999). *Aluminium Handbook1.* Aluminium-Verlag Marketing & Kommunikation GmbH

Liu, G.R. & Gu, Y.T. (2005). *An Introduction to Meshfree Methods and Their Programming,* Springer, Dordrecht

Lorbiecka, A.Z.; Vertnik, R., Gjerkeš, H.; Manojlović, G.; Senčič, B.; Cesar, J. & Šarler, B. (2009): Numerical modelling of Grain Structure in Continuous Casting of Steel. *Computers, Materials & Continua,* Vol. 8, No. 3, pp. 195-208

Lorbiecka, A.Z.& Šarler, B. (2009). Modelling grain growth processes by the conventional Cellular Automata and New Point Automata method. In: G. Tsatsaronis and A. Boyano (ed) *International conference of Optimization Using Exergy- based Methods and Computational Fluid Dynamics*, Berlin, Germany, pp.243-252

Lorbiecka, A.Z.& Šarler, B. (2009). Point automata method for prediction of grain structure in the continuous casting of steel. In: L. Andreas (ed) *3nd International Conference of Simulation and Modelling of Metallurgical Processes in Steelmaking, Steelsim 2009*, ASMET, Leoben, Austria, pp. 192-197

Lorbiecka, A.Z. & Šarler, B. (2010). Simulation of dendritic growth with different orientation by using the point automata method. *CMC: Computers, Materials & Continua,* Vol. 18, No.1, pp. 69-104.

Midownik, M.A. (2002). A review of microstructural computer models used to simulate grain growth and recrystallisation in aluminium alloys. *J.Light. Met*, Vol.2, No.3, pp. 125-135

Nastac, L. (2004). *Modeling and Simulation of Microstructure Evolution in Solidifying Alloys*. Kluwer Academic Publishers

Nakagawa, M.; Narsume, Y.; Ohsasa, K. (2006): Dendrite Growth Model Rusing Front Tracking Technique with New Growth Algorithm. *ISIJ International*, Vol.46, No.6, pp. 909-913

Neumann, J.V. (1987). The general and logical theory of automata, 1963. In: W. Aspray and A. Burks, Editors, *Chapters of John von Neumann on Computing and Computer Theory. The Charles Babbage Institute Reprint Series for the History of Computing,* Vol.12, pp. 477-490

Rappaz, M. & Gandin, Ch.A. (1993). Probabilistic modeling of microstructure formation in solidification processes. *Acta Metall.*, Vol.41, pp. 345-360

Rettenmayr, M.; Buchmann, M. (2006): Solidification and Melting - Asymmetries and Consequences. *Materials Science Forum.*, Vol.508, pp. 205-210

Saito, Y. Goldbeck-Wood, G. & Muller-Krumbhaar, H. (1988). Numerical simulation of dendritic growth. *Physical Review*, Vol. 33, pp. 2148-2157.

Sasikumar, R. & Sreenivasan, R. (1994). Two-dimensional simulation of dendrite morphology. *Acta metall. mater*, Vol.42, No.7, pp. 2381-2386.

Shin, Y.H. & Hong, C.P. (2002). Modeling of Dendritic Growth with Convection Using a Modified Cellular Automata Model with a Diffuse Interface. *ISIJ International*, Vol. 42, No.4, pp. 359-367

Spittle, J.A. & Brown, S.G.R. (1989). Computer simulation of the effect of alloy variable on the grain structures of castings. *Acta. Metall.*, Vol.37, pp. 1803-1810

Spittle, J.A. & Brown, S.G.R. (1995). A cellular automaton model of steady state columnar dendritic growth in binary alloys. *J.Mater. Sci*, vol. 30, pp. 3989-3994

Stefanescu, D. M. (2009). *Science and Engineering of Casting Solidification*. Springer Science

Šarler, B.; Vertnik, R. & Perko, J. (2005). Application of diffuse approximate method in convective diffusive solidification problems, *Computers, Materials & Continua,* Vol. 2, pp. 77-83

Šarler, B. & Vertnik, R. (2006). Meshfree local radial basis function collocation method for diffusion problems. *Computers and Mathematics with Application*, Vol.51, pp. 1269-1282

Qin, R.S. & Wallach, E.R. (2003). A phase-field model coupled with a thermodynamic database. *Acta Materialia*, Vol.51, pp. 6199-6210

Wolfram, S. (2002). *A New Kind of Science.* Wolfram Media, Inc

Voller, V.R. (2008). An enthalpy method for modeling dendritic growth in a binary alloy. *Science Direct, International Journal of Heat and Mass Transfer*, Vol.52, pp. 823-834

Xu, Q.; Li, B.; Liu, Y. & Liu, B. (2008). Numerical modelling of microstructure evolution and dendrite growth in alloy solidification process. *International Journal of Materials and Product Technology*, Vol.33, pp. 37-49

Xu, Q.Y. & Liu, B.C. (2001). Modeling of As-Cast Microstructure of Al Alloy with a Modified Cellular Automaton Method. *Materials Transactions*, Vol.42, No.11, pp. 2316-2321

Zhan, Z.; Wei, Y. & Dong, D. (2008). Cellular automaton simulation of grain growth with different orientation angles during solidification process. *Journal of Materials Processing Technology*, Vol.208, No.1, pp. 1-8

Zhu, M.F. & Hong, C.P. (2001). A modified cellular automaton model for the simulation of dendritic growth in solidification of alloys. *ISIJ International*, Vol.41, No.5, pp. 436-445

Cellular Automata - Innovative Modelling for Science and Engineering

Edited by Dr. Alejandro Salcido

ISBN 978-953-307-172-5
Hard cover, 426 pages
Publisher InTech
Published online 11, April, 2011
Published in print edition April, 2011

Modelling and simulation are disciplines of major importance for science and engineering. There is no science without models, and simulation has nowadays become a very useful tool, sometimes unavoidable, for development of both science and engineering. The main attractive feature of cellular automata is that, in spite of their conceptual simplicity which allows an easiness of implementation for computer simulation, as a detailed and complete mathematical analysis in principle, they are able to exhibit a wide variety of amazingly complex behaviour. This feature of cellular automata has attracted the researchers' attention from a wide variety of divergent fields of the exact disciplines of science and engineering, but also of the social sciences, and sometimes beyond. The collective complex behaviour of numerous systems, which emerge from the interaction of a multitude of simple individuals, is being conveniently modelled and simulated with cellular automata for very different purposes. In this book, a number of innovative applications of cellular automata models in the fields of Quantum Computing, Materials Science, Cryptography and Coding, and Robotics and Image Processing are presented.

How to reference

In order to correctly reference this scholarly work, feel free to copy and paste the following:

Agnieszka Zuzanna Lorbiecka and Božidar Šarler (2011). Point Automata Method for Dendritic Growth, Cellular Automata - Innovative Modelling for Science and Engineering, Dr. Alejandro Salcido (Ed.), ISBN: 978-953-307-172-5, InTech, Available from: http://www.intechopen.com/books/cellular-automata-innovative-modelling-for-science-and-engineering/point-automata-method-for-dendritic-growth

INTECH
open science | open minds

InTech Europe
University Campus STeP Ri
Slavka Krautzeka 83/A
51000 Rijeka, Croatia
Phone: +385 (51) 770 447
Fax: +385 (51) 686 166
www.intechopen.com

InTech China
Unit 405, Office Block, Hotel Equatorial Shanghai
No.65, Yan An Road (West), Shanghai, 200040, China
中国上海市延安西路65号上海国际贵都大饭店办公楼405单元
Phone: +86-21-62489820
Fax: +86-21-62489821